

## RESEARCH ARTICLE

10.1002/2015JC010800

## Seasonal variation of the upper ocean responding to surface heating in the North Pacific

Eunjeong Lee<sup>1</sup>, Yign Noh<sup>1</sup>, Bo Qiu<sup>2</sup>, and Sang-Wook Yeh<sup>3</sup><sup>1</sup>Department of Atmospheric Sciences, Yonsei University, Seoul, South Korea, <sup>2</sup>Department of Oceanography, University of Hawaii, Honolulu, Hawaii, USA, <sup>3</sup>Department of Marine Science and Convergent Technology, Hanyang University, Ansan, South Korea

## Key Points:

- The scaling of MLD under surface heating is obtained by analyzing Argo data
- A large amount of heat flux across MLD is found during summer
- The heat budget of the upper ocean during summer is estimated

## Correspondence to:

Y. Noh,  
noh@yonsei.ac.kr

## Citation:

Lee, E., Y. Noh, B. Qiu, and S.-W. Yeh (2015), Seasonal variation of the upper ocean responding to surface heating in the North Pacific, *J. Geophys. Res. Oceans*, 120, 5631–5647, doi:10.1002/2015JC010800.

Received 24 FEB 2015

Accepted 20 JUL 2015

Accepted article online 23 JUL 2015

Published online 14 AUG 2015

**Abstract** Seasonal variations of the upper ocean, such as mixed layer depth (MLD) and sea surface temperature (SST), responding to the atmospheric forcing in the North Pacific (10°N–50°N), are investigated by analyzing the Argo and NCEP/NCAR reanalysis 1 data. The OAF flux data are also used for comparison. During the early heating period in the high-latitude ocean north of 30°N, where a seasonal thermocline is formed above the deep mixed layer under strong surface heating, the MLD  $h$  is found to be scaled as  $h \propto (L\lambda)^{1/2}$ , where  $L$  is the Monin-Obukhov length scale and  $\lambda$  is the Ekman length scale. On the other hand, in the low-latitude ocean south of 30°N, where the preexisting MLD is shallow and surface heating is weak,  $h$  is found to be scaled by  $\lambda$ . It is found that a large amount of heat flux across the MLD occurs, especially in the high-latitude ocean during the late heating period, in which  $h$  is small. It suggests the contribution by turbulent mixing across the MLD in addition to radiation penetration, and the eddy diffusivity in the high-latitude ocean is estimated as  $K_v \sim 10^{-4} - 10^{-3} \text{ m}^2 \text{ s}^{-1}$ . The heat budget of the mixed layer reveals that the contribution from the ocean heat transport is much smaller than the surface heat flux in the high-latitude ocean except in the Kuroshio region, but it is sometimes comparable in the low-latitude ocean.

## 1. Introduction

Variation of the sea surface temperature (SST) in response to the atmospheric forcing plays a critical role in the climate system, as it controls the exchange of heat and moisture between the atmosphere and the ocean. The increase of SST under surface heating is determined by how much heat flux enters through the sea surface, how deep the surface heat flux penetrates downward, and how much heat is transported horizontally in the ocean. Meanwhile, how deep the surface flux penetrates downward is determined by the mixed layer depth (MLD) and the heat flux across the MLD.

During winter, the MLD grows by convection, which entrains deeper water. On the other hand, during summer, the balance between turbulent kinetic energy (TKE) generation by wind stress and its decay by surface heating leads to the formation of a seasonal thermocline at shallower depths, and determines the MLD in general.

Regarding the depth of a seasonal thermocline, Kraus and Turner [1967] suggested the Monin-Obukhov length scale  $L (= u_*^3/B_0)$ , where  $B_0$  is the surface buoyancy flux and  $u_*$  is the frictional velocity, and this scale has been used in many previous studies to estimate the MLD, or  $h$ , during summer. Meanwhile, the scaling of  $h$  by  $L$  was found to overestimate  $h$  in the midlatitudes [Alexander and Kim, 1976], and modifications were suggested to rectify this problem by including the effect of the Coriolis force [Resnyanskiy, 1975; Elsberry et al., 1976; Garwood, 1977; Wells, 1979; Gaspar, 1988]. Recently, Goh and Noh [2013] showed that the depth of a seasonal thermocline is proportional to  $(L\lambda)^{1/2}$  using the large eddy simulation (LES), where  $\lambda$  is the Ekman length scale ( $= u_*/f$ ) and  $f$  is the Coriolis parameter. This scaling  $h \propto (L\lambda)^{1/2}$  was confirmed by Yoshikawa [2015] who analyzed Argo data with decreasing MLD in late spring. He also suggested that  $h$  tends to be scaled by  $\lambda$ , when  $\lambda$  becomes smaller than  $L$ . The scaling based on  $(L\lambda)^{1/2}$  was also suggested by Nieuwstadt [1984] and Zilitinkevich et al. [2007] to estimate the equilibrium depth of the stable boundary layer in the atmosphere.

Many studies have reported the distribution of MLD in the global ocean with seasonal and interannual variations based on various sources of observational data and model results [Kara et al., 2003; de Boyer

Montégut *et al.*, 2004; Carton *et al.*, 2008; Noh and Lee, 2008; Ohno *et al.*, 2009]. By and large, these studies focused on the winter mixed layer, in which the variation of MLD is large. Only a few studies considered the upper ocean response, such as MLD, to surface heating [Alexander and Kim, 1976; Schneider and Müller, 1990; Yu *et al.*, 2006; Hao *et al.*, 2012; Cronin *et al.*, 2013; Hosoda *et al.*, 2015].

The heat flux across the base of the ML is often neglected during the heating season [Yu *et al.*, 2006], based on the assumption used in bulk models that no entrainment occurs at the MLD, when equilibrium is reached under surface heating [Kraus and Turner, 1967; Gaspar, 1988]. Meanwhile, a recent work reveals that a large amount of heat flux across the base of the mixed layer (ML) occurs in the North Pacific Ocean during summer [Qiu *et al.*, 2006; Cronin *et al.*, 2013; Hosoda *et al.*, 2015]. Alexander *et al.* [2000] and Vivier *et al.* [2002] also suggested that entrainment arising from day-to-day changes of MLD can contribute to the heat flux across the monthly mean MLD.

How much heat is transported horizontally in the ocean is usually investigated by the heat budget analysis of the ML [Qiu and Kelly, 1993; Deser *et al.*, 1996; Alexander *et al.*, 2000; Yasuda *et al.*, 2000; Tomita *et al.*, 2002; Vivier *et al.*, 2002; Qu, 2003; Kelly, 2004; Qiu *et al.*, 2004; Dong *et al.*, 2007; Kako and Kubota, 2009; Kang *et al.*, 2010]. Although many of them investigated the heating season as well, most of the results are based on mixed layer model results, and thus affected by the uncertainties of the model prediction.

Unlike during winter, the heat budget of the ML during summer is found to be dominated by the surface heat flux, and the contribution from horizontal heat transport is often negligible, because of the shallower MLD and smaller horizontal temperature gradient [Qiu and Kelly, 1993; Qu, 2003; Liu *et al.*, 2005].

With an aim to understand how much SST increases responding to surface heating, we attempt to address three critical questions in the present paper: (1) how deep the MLD is, (2) how much heat flux occurs across the MLD, and (3) how much horizontal heat transport contributes to the heat budget of the ML. For this purpose, we investigate the variations of MLD, SST, heat content, and the heat flux across the MLD in the North Pacific, in response to surface heating, by analyzing observation data.

## 2. Data and Methods

The following two data sets were used in the present study; the Argo data set for temperature profiles in the upper ocean [Argo Science Team, 2001] and the National Center for Environmental Prediction/National Center for Atmospheric Research (NCEP/NCAR) reanalysis 1 data set (NCEP-1) for the surface heat flux and wind stresses [Kalnay *et al.*, 1996]. Over 100,000 units of Argo profile data are produced each year since 1998, subject to consistent quality control. The accuracies of temperature, salinity, and pressure sensors on the Argo floats are  $\pm 0.005^\circ\text{C}$ ,  $\pm 0.01$  psu, and  $\pm 2.4$  dbar, respectively. The NCEP-1 data provide both wind stress and heat flux data during the period corresponding to the Argo data (1998–2007). The Argo and NCEP-1 data were used together in many previous works [Ohno *et al.*, 2004; Dong *et al.*, 2007; Holte *et al.*, 2012]. In order to examine how the results can be affected by the surface heat flux data, we also compared the results using the heat flux from the Objectively Analyzed Air-Sea Fluxes (OAFlux) data [Yu *et al.*, 2004]. The NCEP-1 data are still used for the wind stress data in this case, however, because the wind stress data are not available yet from the OAFlux data.

The domain of analysis was the latitudinal zone of  $10^\circ\text{N}$ – $50^\circ\text{N}$  in the North Pacific. For analysis, the monthly mean data in the period from 1998 to 2007 were obtained from both Argo and NCEP-1, and remapped by multilinear interpolation with a  $2^\circ \times 2^\circ$  spatial resolution. Temperature data from each Argo profile within a grid cell were interpolated to a profile with 5 m intervals, and MLD was calculated from individual profiles, before the spatial and temporal averages were carried out.

The remapping filtered out the signals of mesoscale eddy variability. The data for MLD were obtained using the criterion of temperature difference from SST by  $0.2^\circ\text{C}$  from each profile, as in Hosoda *et al.* [2010]. The MLD data based on the criterion by  $0.5^\circ\text{C}$  were also obtained for comparison. Here the temperature at  $z = 5$  m was regarded as SST. Data were analyzed for the period during April–August, corresponding to the heating season in the North Pacific, and the data with negative surface heat flux were eliminated.

The surface buoyancy flux  $B_0$  is calculated by  $B_0 = (g/\rho)(\alpha Q_0/c_p + \beta S_0 H_0)$ , where  $Q_0$  is the surface heat flux,  $H_0$  is the surface freshwater flux,  $\alpha \equiv -\rho^{-1}\partial\rho/\partial T$ ,  $\beta \equiv \rho^{-1}\partial\rho/\partial S$ ,  $\rho$  is density,  $g$  is gravitational

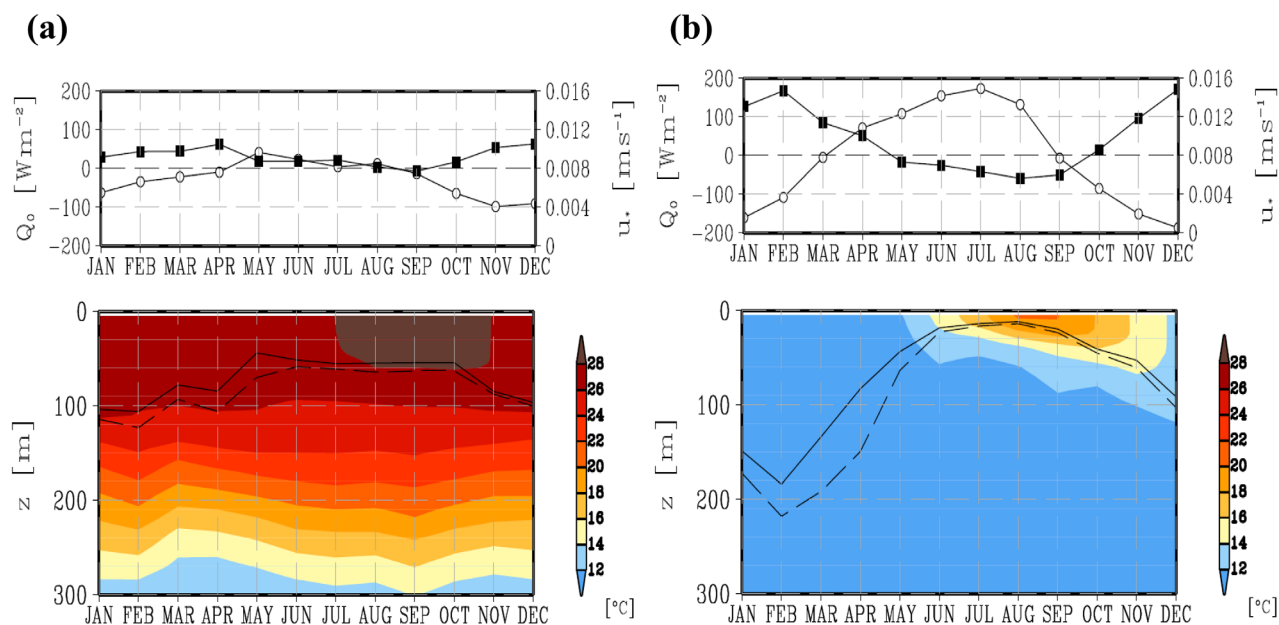


**Figure 1.** Seasonal variations of surface heat flux (open circle), frictional velocity (filled square), and vertical temperature profiles (colored shades). Also plotted are the variations of  $h$ , obtained from the two different temperature criteria (solid:  $\Delta T = 0.2^\circ C$ , dashed:  $\Delta T = 0.5^\circ C$ ). (a)  $15^\circ N$ ,  $180^\circ E$ , (b)  $40^\circ N$ ,  $180^\circ E$ .

acceleration,  $S_0$  is the surface salinity, and  $c_p$  is the heat capacity of sea water. Contributions from  $H_0$  to  $B_0$ , and the effect of salinity on the determination of MLD are neglected in the present analysis, as they are expected to be insignificant during summer in most regions of our interest. Sensitivity tests are carried out to examine these effects, however.

### 3. Results

#### 3.1. Seasonal Variation of the Upper Ocean and the Atmospheric Forcing

In order to understand the general feature of the upper ocean response to the atmospheric forcing, we plot the seasonal variations of surface heating ( $Q_0$ ), the frictional velocity ( $u_*$ ), and temperature ( $T$ ) profiles at high and low latitudes ( $\phi = 15^\circ N$  and  $40^\circ N$ ) in Figure 1. Superimposed on the temperature profiles are the variations of MLD, obtained with the temperature difference from SST by  $0.2^\circ C$  and  $0.5^\circ C$ .

The seasonal variation of the mixed layer shows a quite different pattern, depending on the latitude. At the high-latitude ocean, strong surface heating leads to the formation of a seasonal thermocline from the deep mixed layer of uniform temperature that is produced by convection during the previous winter. The MLD,  $h$ , decreases significantly with time until June as surface heating increases. It does not vary much thereafter until August, but temperature continues to increase, not only within the ML, but also below  $h$ , indicating the heat flux across MLD. On the other hand, in the low latitude, MLD is shallower than 100 m throughout the year, and only a small decrease of  $h$  is observed after the start of surface heating in May. Surface heating is much weaker compared to that in the high-latitude ocean. Figure 1 also shows that  $h$  obtained from the different criteria of temperature difference from SST ( $0.2^\circ C$  versus  $0.5^\circ C$ ) is almost identical in summer, although they differ in winter.

Latitudinal contrast can be clearly identified in the distributions of atmospheric forcing and MLD in May and July (Figure 2). Surface heating is stronger in the high-latitude ocean ( $\phi > 30^\circ N$ ), and weaker in the low-latitude ocean ( $\phi < 30^\circ N$ ), which reflects a large SST difference between two regions. Meanwhile, wind stress is weaker in the high-latitude ocean, and stronger in the low-latitude ocean. Accordingly, MLD decreases greatly in the high-latitude ocean, but it does not vary significantly in the low-latitude ocean. Figure 3a indeed shows that the rapid decrease of  $h$  larger than 60 m occurs only in the high-latitude ocean north of  $30^\circ N$  during the early period of surface heating (March–June). The rapid decrease of  $h$  does not occur any more even in the high-latitude ocean, however, during the later period of surface heating (June–August) (Figure 3b). Figures 2 and 3 also show that the boundary between the high-latitude and

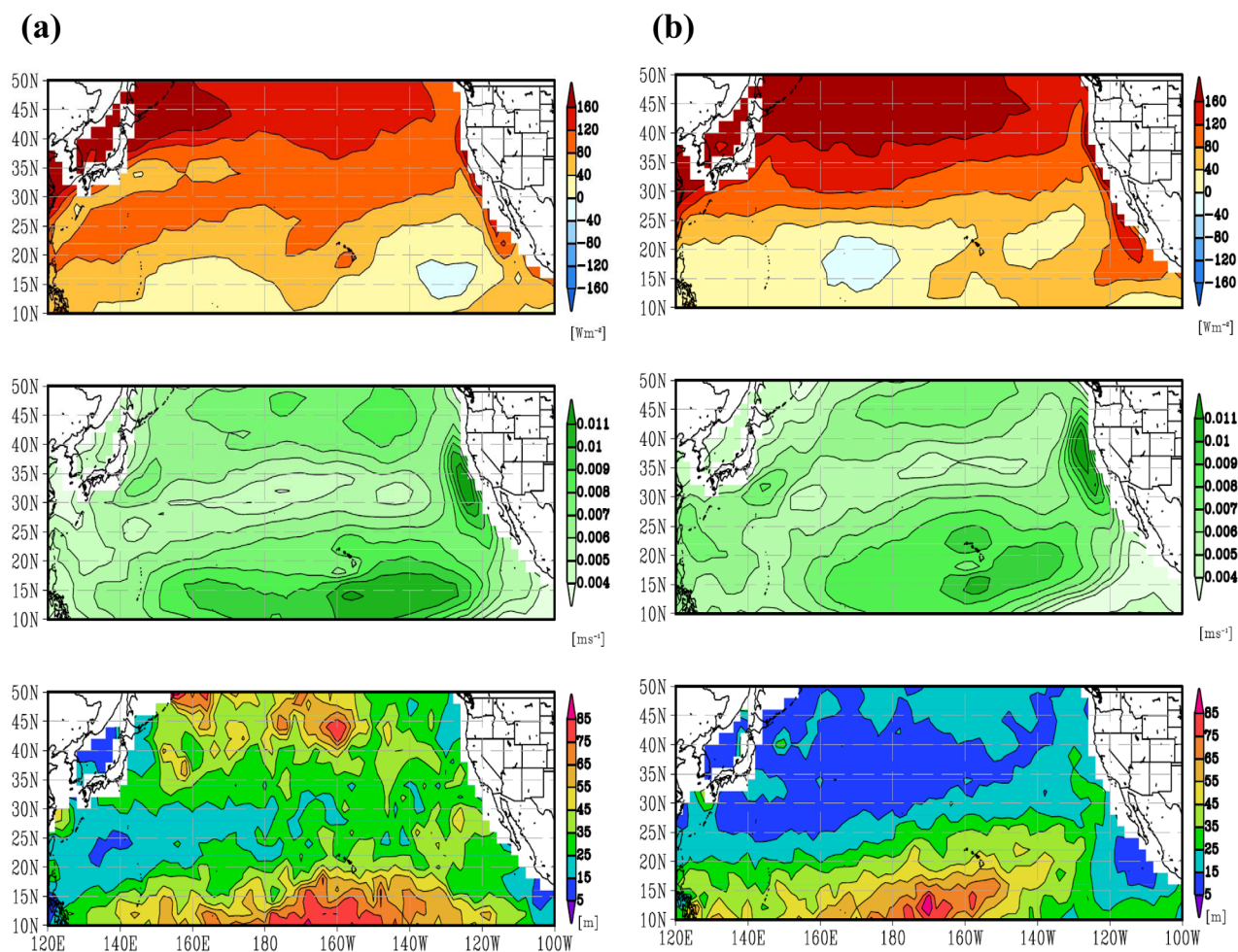


Figure 2. Distributions of the (top) downward surface heat flux, (middle) frictional velocity, and (bottom)  $h$ . (a) May and (b) July.

low-latitude regimes tends to shift slightly northeastward, especially in the ocean along the west coast of North America, reflecting weaker seasonal variation of the atmospheric forcing there.

This suggests the possibility that the dynamical process controlling the upper ocean variation may be different between the high-latitude and low-latitude oceans. Theories of the seasonal thermocline formation [Kraus and Turner, 1967; Goh and Noh, 2013] considered the situation in which a seasonal thermocline is formed under surface heating from the well-mixed layer without stratification. This condition is well satisfied during the early period of surface heating in the high-latitude ocean. On the other hand, in the

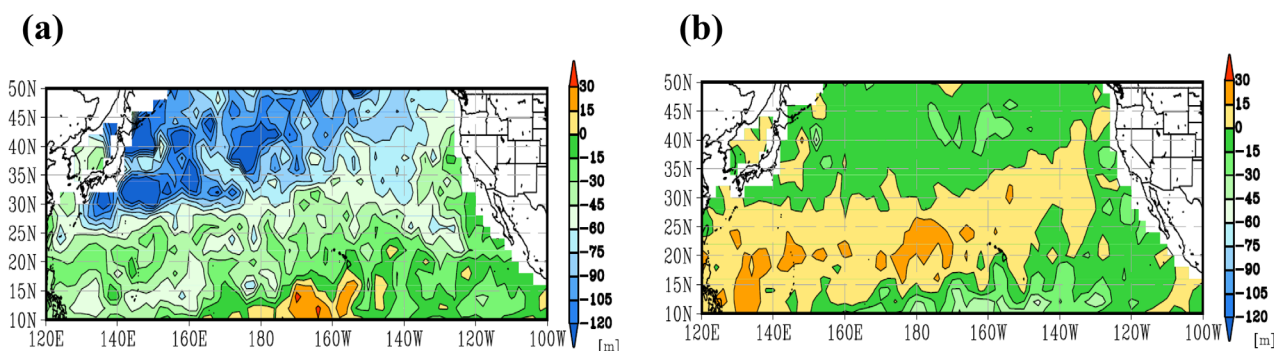
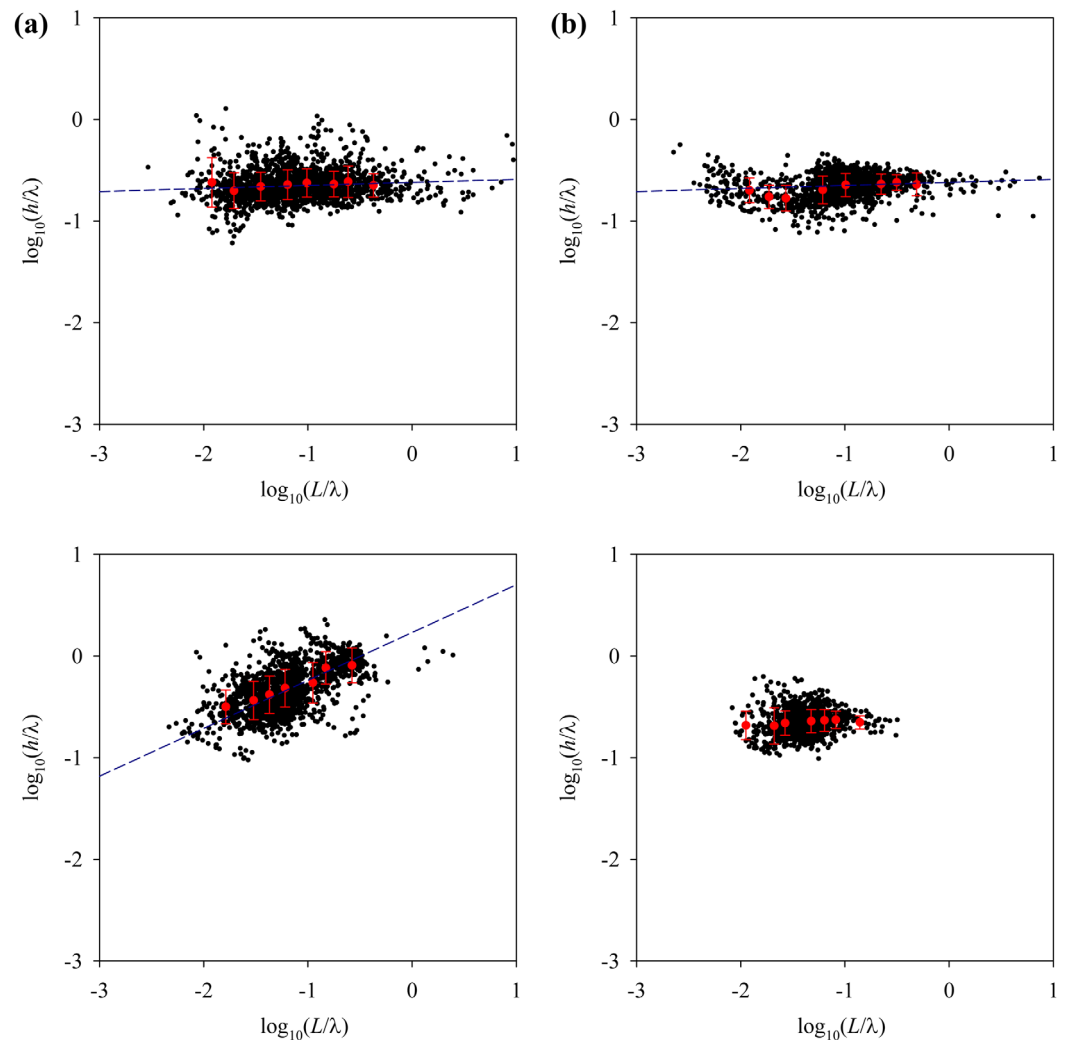


Figure 3. Distributions of the difference of  $h$  from (a) March to June and (b) June to August.



**Figure 4.** Scatter plots between  $h/\lambda$  and  $L/\lambda$  in the domains of (top)  $\phi < 30^\circ\text{N}$  and (bottom)  $\phi > 30^\circ\text{N}$ . Red circles with vertical bar represent average and standard deviation of  $h/\lambda$ . Dashed lines represent the regression line, corresponding to Table 1. (a) April–June and (b) July–August.

low-latitude ocean, stratification, or a thermocline, already exists in shallow depths, probably shallower than the depth at which a seasonal thermocline is supposed to form from the well-mixed layer under the condition of weak surface heating and strong wind stress. As a result, the response of the upper ocean to surface heating, or the formation of a seasonal thermocline, can be strongly affected by the preexisting thermocline in the upper ocean.

### 3.2. The Mixed Layer Depth

If the depth of a seasonal thermocline, or equivalently the MLD during the heating season,  $h$  is determined by  $f$  as well as  $u_*$  and  $B_0$ , if the initial temperature profile is uniform. Dimensional analysis leads to the relation

$$h/\lambda = \Phi(L/\lambda). \quad (1)$$

For example, the scaling of  $h$  as  $h \propto L$  [Kraus and Turner, 1967] and  $h \propto (L\lambda)^{1/2}$  [Goh and Noh, 2013] correspond to  $h/\lambda \propto (L/\lambda)^\gamma$  with  $\gamma = 1$  and  $1/2$ , respectively.

Considering the different characteristics of the upper ocean response to surface heating, as shown in Figures 1–3, we plot the scatter plots of  $h/\lambda$  versus  $L/\lambda$  for four groups of data (the early heating period versus the late heating period, and the high-latitude ocean versus the low-latitude ocean) (Figure 4). Here in order to help identify the characteristics of the high-latitude and low-latitude oceans more clearly, the data with

small MLD decrease from March to June ( $|\Delta h| < 30$  m) in the high-latitude ocean, and the data with large MLD decrease ( $|\Delta h| > 60$  m) in the low-latitude ocean, shown in Figure 3, are filtered out.

Figure 4 shows that the relation  $h \propto (L\lambda)^{1/2}$ , predicted by Goh and Noh [2013], can be observed only during the early heating period in the high-latitude ocean. In other cases the data are better represented by the relation  $h \propto \lambda$ . For example, for the relation  $h/\lambda = A(L/\lambda)^\beta$ , or  $h = AL^\beta \lambda^{(1-\beta)}$ , the linear regression gives  $A = 1.71$  and  $\beta = 0.47$  during the early heating season in the high-latitude ocean with the standard error of estimate (SE) 0.14 m, and  $A = 0.24$  and  $\beta = 0.03$  is obtained with SE = 0.13 m during the whole heating period in the low-latitude ocean. The proportional constant in the relation  $h = A(L\lambda)^{1/2}$  from observation data ( $A = 1.71$ ) is larger than LES results ( $A = 0.5$ ) from Goh and Noh [2013], probably because of the large difference between the data sets in temporal and spatial resolutions (e.g., monthly mean data in the present case), in the methods of calculating MLD, and the absence of the heat flux across the MLD in LES. The relation  $h \propto L$ , suggested by Kraus and Turner [1967], is not found anywhere in Figure 4, and therefore the possibility of this scaling is clearly excluded.

Yoshikawa [2015] also found the relation  $h \propto (L\lambda)^{1/2}$ , when he analyzed the data of decreasing MLD in late spring, under the condition that  $B_0$  is larger than a critical value and increasing with time and  $u_*$  decreasing with time. It precluded the data leading to the relation corresponding to  $h \propto \lambda$  in Figure 4. On the other hand, Lozovatsky et al. [2005] obtained the relation  $h \cong 0.44\lambda$  in spring in the Atlantic Ocean near 53°N, in which the contribution from surface heating is much smaller than that from wind stress in the TKE budget of the ML.

Our present results reveal that the idealized formation of a seasonal thermocline from the well-mixed upper ocean under surface heating, which was considered in the mixed layer model [Kraus and Turner 1967] or in LES [Goh and Noh 2013], is relevant only in the high-latitude ocean, especially in the early period of surface heating. In the low-latitude ocean, a thermocline already exists above the depth at which a seasonal thermocline is supposed to form under the surface heat flux and wind stress. It is found indeed that the predicted depth of a seasonal thermocline, calculated by  $h = AL^\beta \lambda^{(1-\beta)}$  with  $A = 1.71$  and  $\beta = 0.47$ , is much deeper than the preexisting MLD in the low-latitude ocean. In this case  $h$  is controlled rather by  $\lambda$ , which represents the vertical extent of the downward transport of the wind stress. The tendency of  $h \propto \lambda$  during the late heating period in the high-latitude ocean also reflects the fact that the MLD already exists at a shallower depth (Figure 4b).

The present result indicates that  $h$  is affected by the value of the preexisting MLD,  $h_0$ , in addition to  $u_*$ ,  $Q_0$ , and  $f$ . In this case the relation for  $h$  can be modified to  $h \propto (L\lambda)^{1/2} \Phi[h_0/(L\lambda)^{1/2}]$ , and the present results can be interpreted as  $h \propto (L\lambda)^{1/2}$  for  $h_0/(L\lambda)^{1/2} \gg 1$ , but  $h \propto h_0 \propto \lambda$  for  $h_0/(L\lambda)^{1/2} \ll 1$ .

If  $h$  is affected by the preexisting thermocline,  $h$  can be affected by the stratification at the thermocline as well. For example, Pollard et al. [1973] suggested that the initial MLD growth by wind mixing can be scaled by  $u_*/(fN)^{1/2}$ , where  $N^2$  is the stratification below the ML. Therefore, we compare the relation of  $h$  with  $\lambda$  and  $u_*/(fN)^{1/2}$  (Figure 5). Here the value of  $N(z = h)$  of the previous month is used so as to represent preexisting stratification. Figure 5 shows that  $h$  is scaled better by  $\lambda$  than by  $u_*/(fN)^{1/2}$ . It is important to mention that the monthly mean MLD does not increase with time during the heating season, and thus the stratification below the MLD may not play an important role in determining  $h$ , contrary to the case of the mixed layer deepening by wind mixing and convection.

In order to examine the robustness of the present results, we performed various sensitivity tests using different analysis methods, and compared the values of  $A$ ,  $\beta$ , and SE with the present analysis (CTL) (Table 1). Experiment A used all data without filtering out the data with large/small  $\Delta h$  in the low-/high-latitude ocean (Figure 3). Experiment B excluded the radiation penetration across the MLD in calculating  $Q_0$ . Experiment C included the contribution of the surface freshwater flux ( $H_0$ ) to  $B_0$ , and determined the MLD by the criterion based on density ( $\Delta\sigma_\theta = 0.03 \text{ kg m}^{-3}$ ) instead of temperature ( $\Delta T = 0.2^\circ\text{C}$ ). Finally, Experiment D used the OAFflux data for heat flux instead of NCEP-1. Table 1 confirms that essentially the same conclusion can be obtained from all these different methods of analysis.

The ratio of the contribution from the surface freshwater flux  $H_0$  to the surface buoyancy flux  $B_0$  is shown in Figure 6. It is found to be negligible in the high-latitude ocean. If a seasonal thermocline (or pycnocline) is formed under surface heating from the deep well-mixed layer generated by winter convection during the previous winter, MLD is expected to be essentially determined by temperature, since the contribution from

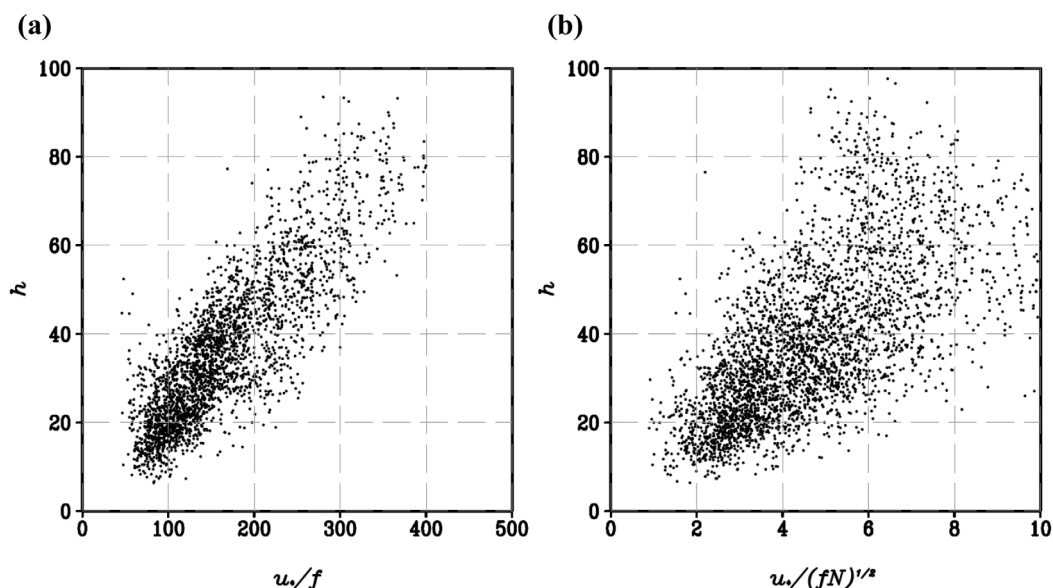


**Figure 5.** Scatter plots between (a)  $h$  and  $\lambda (= u_* / f)$  and (b)  $h$  and  $u_* / (fN)^{1/2}$  in the low-latitude ocean ( $\phi < 30^\circ\text{N}$ ).

$H_0$  is negligible. On the other hand, in the low-latitude ocean  $H_0$  contributes to  $B_0$  significantly, mainly because the magnitude of  $Q_0$  is very small (Figure 2). Nonetheless, the MLD in this region is not affected by  $B_0$ , as shown in Figure 4, and the relation  $h \propto \lambda$  remains valid.

### 3.3. Heat Budget of the Upper Ocean

Figure 7 shows the distribution of monthly temperature increase at different depths down to  $z = 100$  m in May and July. In both cases, the downward heat transport from the sea surface reaches deeper in the Kuroshio Extension region where the subsurface shear associated with the Kuroshio generates vertical mixing over a much deeper depth [Noh and Lee 2008]. The distribution of  $\Delta T(z = 60 \text{ m})$  in July suggests deeper penetration of heat in the latitudinal zone ( $20^\circ\text{N}$ – $30^\circ\text{N}$ ) in the central Pacific, reflecting the deeper MLD there (Figure 2). In the lower latitude ( $\phi < 20^\circ\text{N}$ ), MLD may be deeper, but the surface heat flux is very weak.

Figure 7 suggests that the downward heat transport from the sea surface in summer is largely limited to  $z = 100$  m in the North Pacific. The domain averaged monthly temperature increase is estimated at each depth ( $z = 5, 30, 60,$  and  $100$  m) as 1.16, 0.79, 0.19, and  $-0.02^\circ\text{C}$  in May, and 1.29, 0.84, 0.11, and  $-0.07^\circ\text{C}$  in July, respectively.

The evolution of vertical profiles of the domain averaged  $\Delta T(z)$  also supports that the downward transport of the surface heat flux does not reach deeper than  $z = 100$  m (Figure 8). In April,  $\Delta T(z)$  decreases continuously with depth from the sea surface, and almost disappears at  $z = 100$  m. The penetration depth decreases with increasing surface heat flux after May. Although small values of  $\Delta T(z)$  reappear below

**Table 1.** Comparison of Regression Coefficients From Different Analysis Methods<sup>a</sup>

	$\phi < 30^\circ\text{N}$			$\phi > 30^\circ\text{N}$		
	A	$\beta$	SE	A	$\beta$	SE
CTL	0.24	0.03	0.13	1.71	0.47	0.14
A	0.24	0.04	0.14	1.59	0.44	0.14
B	0.24	0.03	0.13	1.70	0.47	0.14
C	0.19	0.05	0.14	1.70	0.42	0.13
D	0.29	0.09	0.12	1.70	0.47	0.14

<sup>a</sup>A is the case with no data filter in the high-latitude and low-latitude ocean, B with the exclusion of radiation penetration across the MLD from  $Q_0$  (water type 2), C with the inclusion of the contribution of the surface freshwater flux to  $B_0$ , and the determination of MLD by  $\Delta\sigma_\theta = 0.03 \text{ kg m}^{-3}$ , D with the OAF flux data used for heat flux instead of NCEP-1. CTL represents the control experiment used for analysis in the present work.

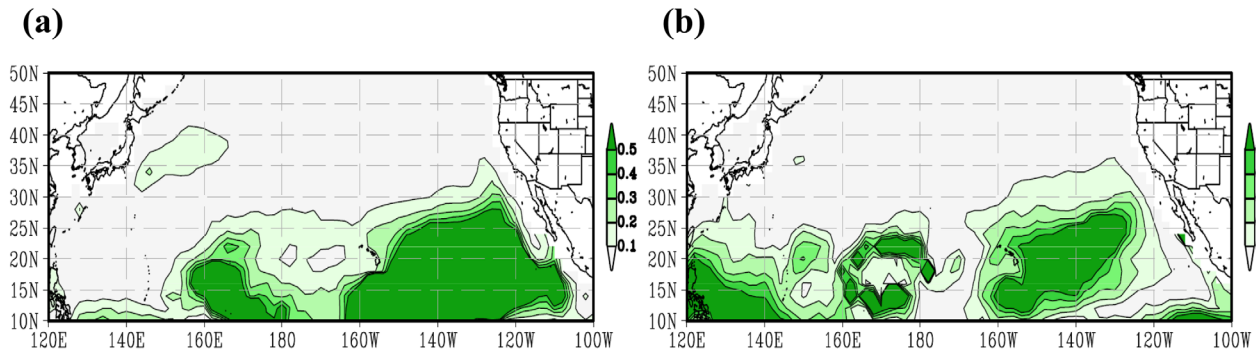


**Figure 6.** Distributions of the ratio of the contribution of the surface freshwater flux to the total surface buoyancy flux. (a) May and (b) July.

$z = 100$  m, its variation does not appear to be related to the variation of surface heating (e.g., the negative  $\Delta T$  during the strongest surface heating in July), suggesting that it is due to other factors such as the seasonal variation of ocean currents.

The heat budget of the ML is expressed by

$$\rho c_p \int_{-h}^0 \frac{\partial T}{\partial t} dz = (Q_0 - Q_h) + \int_{-h}^0 F dz. \quad (2)$$

Here  $F$  is the contributions from the horizontal heat flux convergence, including the advection by geostrophic and Ekman velocity and turbulent diffusion,  $Q_h$  is the heat flux across the MLD at  $z = h$ . The heat flux across the MLD is usually assumed to occur by entrainment during the growth of MLD under surface cooling, and thus estimated by  $Q_h = \rho c_p w_e \Delta T$ , where  $w_e$  is the entrainment rate and  $\Delta T (= T_m - T_o)$  is the difference of temperature in the ML ( $T_m$ ) and below the ML ( $T_o$ ). On the other hand,  $Q_h$  is not yet estimated properly during the heating season, although it is often assumed to be zero based on  $w_e = 0$  as in the bulk mixed layer models [Kraus and Turner, 1967; Gaspar, 1988]. However, Figures 1 and 7 suggest that a large amount of heat is transferred to below the MLD under surface heating, thus  $Q_h$  cannot be neglected. Hereafter we refer the terms in the LHS of (2) as HCV (heat content variation),  $Q_0$  as SHF (surface heat flux), and the last terms in the RHS of (2) as OHT (ocean heat transport). All variables represent the monthly mean values.

It is difficult to evaluate  $Q_h$  in (2). On the other hand, Figures 7 and 8 indicate that the heat flux almost disappears at  $z = 100$  m, so we consider the heat budget over the water column down to  $z = 100$  m, instead of down to  $z = h$ . In this case (2) is rewritten as

$$\rho c_p \int_{-z_H}^0 \frac{\partial T}{\partial t} dz = Q_0 + \int_{-z_H}^0 F dz, \quad (3)$$

with  $z_H = 100$  m. Here  $z_H$  represents the maximum depth of the downward penetration of surface heating, and thus the minimum depth with no vertical heat transport. We will refer the last term in the RHS of (3) as OHT<sub>zH</sub>. Equation (3) allows us to calculate OHT<sub>zH</sub> by the difference of the other two terms. The temperatures at the start and the end of the month, which is used to calculate  $\partial T / \partial t$  in (3), are obtained from the average of two monthly temperatures. The domain average of (3), as in Figure 8, gives that monthly mean of the increase of heat content and the SHF for three months from May to July are evaluated as  $79.92 \text{ Wm}^{-2}$  and  $78.68 \text{ Wm}^{-2}$ , respectively. It supports further the assumption of no heat transport across  $z = 100$  m, if the heat transport across the lateral boundary across the whole domain is neglected.

Among the contributions to the ocean heat transport, the advection by geostrophic and Ekman velocity and turbulent diffusion, the contribution from Ekman advection, EKA, can be obtained directly from the wind stress field [e.g., Tomita et al., 2002; Kang et al., 2010], as

$$\rho c_p \mathbf{U}_E \cdot \nabla T_m, \quad (4)$$

where  $\mathbf{U}_E = \boldsymbol{\tau} \times \mathbf{k} / (\rho f)$ ,  $\boldsymbol{\tau}$  is the surface wind stress vector, and  $\mathbf{k}$  is the vertical unit vector. Figure 9 shows mainly negative and positive contributions from EKA in the high-latitude and low-latitude ocean in

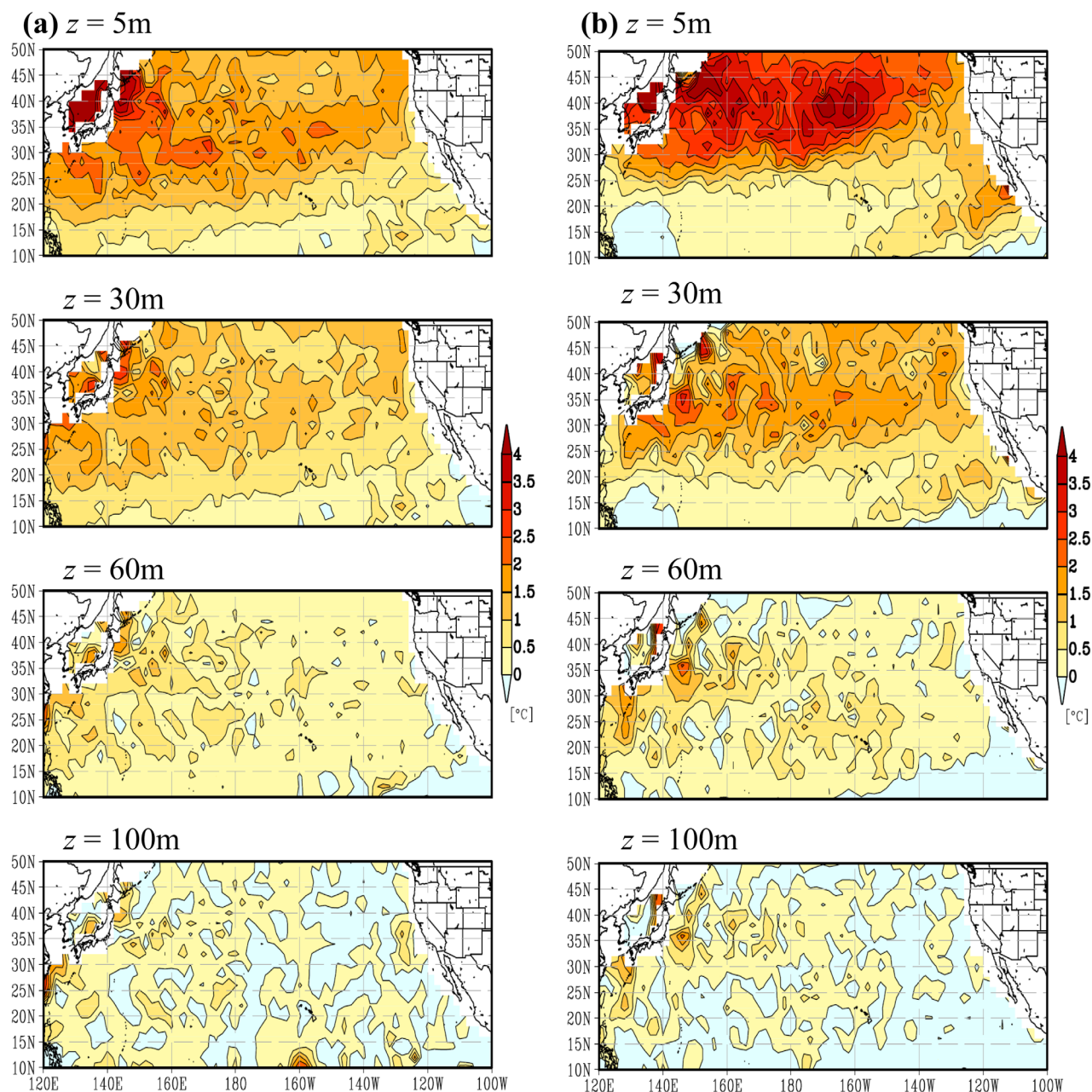


**Figure 7.** Distributions of temperature increase at  $z = 5, 30, 60,$  and  $100$  m. (a) May and (b) July.

accordance with the dominant wind direction, but their magnitudes are much smaller than SHF. Table 2 indicates that the domain averaged contribution from EKA is only about 7.6% and 4.1% of that from SHF in May and July in the high-latitude ocean.

Contrary to the vertical component of turbulent velocity responsible for vertical mixing, the horizontal components of mean and turbulent velocity responsible for advection and lateral mixing are not affected by stratification directly. Therefore, geostrophic advection and lateral diffusion by mesoscale eddies are expected to be insensitive to stratification or MLD. Especially in the Kuroshio region, in which the contribution of the ocean heat transport is the largest, the depth scales of both the Kuroshio and mesoscale eddies in the KE region are larger than 100 m, regardless of season [Kagimoto and Yamagata, 1997; Qiu and Chen, 2005; Yim *et al.*, 2010]. Furthermore, the vertical variation of horizontal temperature gradients down to  $z = 100$  m is usually much smaller than the horizontal temperature gradient itself. As a result, one can

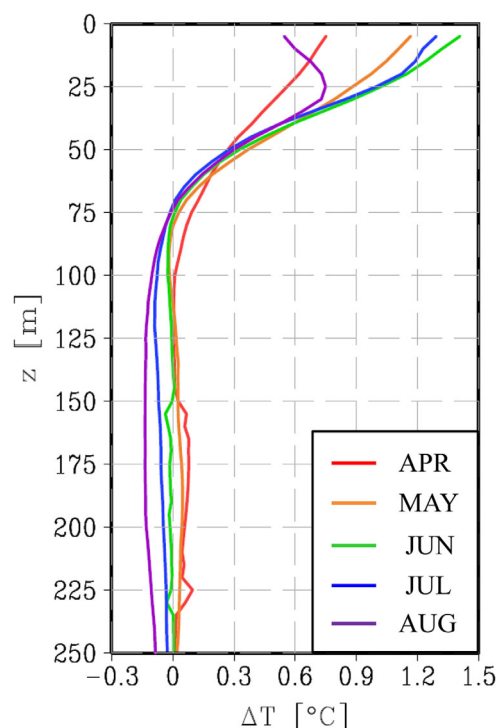


**Figure 8.** Evolution of vertical profiles of the domain-averaged  $\Delta T(z)$  from April to August.

summer in the mixed layer in the western North Pacific, because of shallower MLD and smaller horizontal temperature gradient [Qiu and Kelly, 1993; Qu, 2003; Liu et al., 2005]. Meanwhile, SHF + OHT is much larger than HCV in July in the high-latitude ocean (Figure 9), suggesting the existence of large  $Q_h$ .

The relation between MLD and the increase of SST, represented by  $\Delta T(z = 5 \text{ m})$  in Figure 7, can be understood from the heat budget analysis discussed above. In the highest latitude ( $40^\circ\text{N}$ – $50^\circ\text{N}$ ),  $\Delta T(z = 5 \text{ m})$  is less than in the lower latitude ( $25^\circ\text{N}$ – $40^\circ\text{N}$ ), in spite of the maximum  $Q_0$ , because of the deeper MLD. On the other hand, higher  $\Delta T(z = 5 \text{ m})$  along the Kuroshio in spite of weaker  $Q_0$  (Figure 2) indicates the contribution from OHT.

If geostrophic advection and turbulent diffusion occur uniformly in the upper ocean, as assumed above, they may not induce stratification in the upper ocean, unlike the surface heat flux, and they may not affect the depth of a seasonal thermocline, which is determined by the balance between turbulent mixing and stratification. On the other hand, Ekman advection can modify the effective surface heat flux  $Q_0$ , as it is limited to the mixed layer. Nonetheless, its magnitude is very small compared to SHF in the high-latitude ocean (Figure 9, Table 2), where  $h$  is expected to be controlled by  $Q_0$ .

### 3.4. Heat Flux Across the Mixed Layer Depth

Figure 1b suggests that a significant amount of heat flux occurs during the late summer in the high-latitude ocean. Figure 7 also shows that surface heat flux penetrates much deeper than MLD. Therefore, it is important to estimate the heat flux across the MLD  $Q_h$ , as well as  $h$  and OHT, in order to predict the increase of SST under surface heating.

Figure 10 shows the distributions of  $Q_h/Q_0$ , where  $Q_h$  is calculated from (2) by residual. It shows that there are many regions with  $Q_h/Q_0 > 0.5$ , especially in most regions of the high-latitude ocean in July. It is a contrast to the cooling period, where  $Q_h$  occurs mainly through the increase of MLD by entrainment. On the other hand,  $Q_h/Q_0$  is generally small in the high-latitude ocean in May, when MLD is deeper, suggesting that the heat flux across the MLD may not be significant during this period. Comparison of Figures 2 and 10 reveals the tendency of large  $Q_h/Q_0$  in the region with shallower MLD. A scatter plot between  $Q_h/Q_0$  and  $h$

expect the vertical variation of the ocean heat transport is small down to  $z = 100 \text{ m}$ , especially in the Kuroshio region. For example, Imawaki et al. [2001] obtained the vertical profile of the Kuroshio transport from observation data, which show that the transport decreases only by 4% from the surface to the depth  $z = 100 \text{ m}$ . On the other hand, Ekman advection is mainly limited to the mixed layer, because the Ekman spiral is limited by the seasonal thermocline [Goh and Noh, 2013]. Based on these features, we assume that the contributions from geostrophic advection and lateral diffusion are uniform in the upper 100 m, and estimate OHT by

$$\text{OHT} = (h/z_H)(\text{OHT}_{zH} - \text{EKA}) + \text{EKA}. \quad (5)$$

Figure 9 shows the distributions OHT obtained in this way, together with SHF, EKA, and HCV. In the high-latitude ocean, OHT is much smaller than SHF except near the Kuroshio region. On the other hand, in the lower latitude, where SHF is small, OHT is often comparable to SHF. Table 2 indicates that the domain averaged  $|\text{OHT}|$  in May and July are only about 15.7% and 8.0% of  $|\text{SHF}|$  in the high-latitude ocean, including the Kuroshio region, whereas they are 36.2% and 35.3% in the low-latitude ocean. Previous analyses also suggested that OHT is much smaller than SHF during

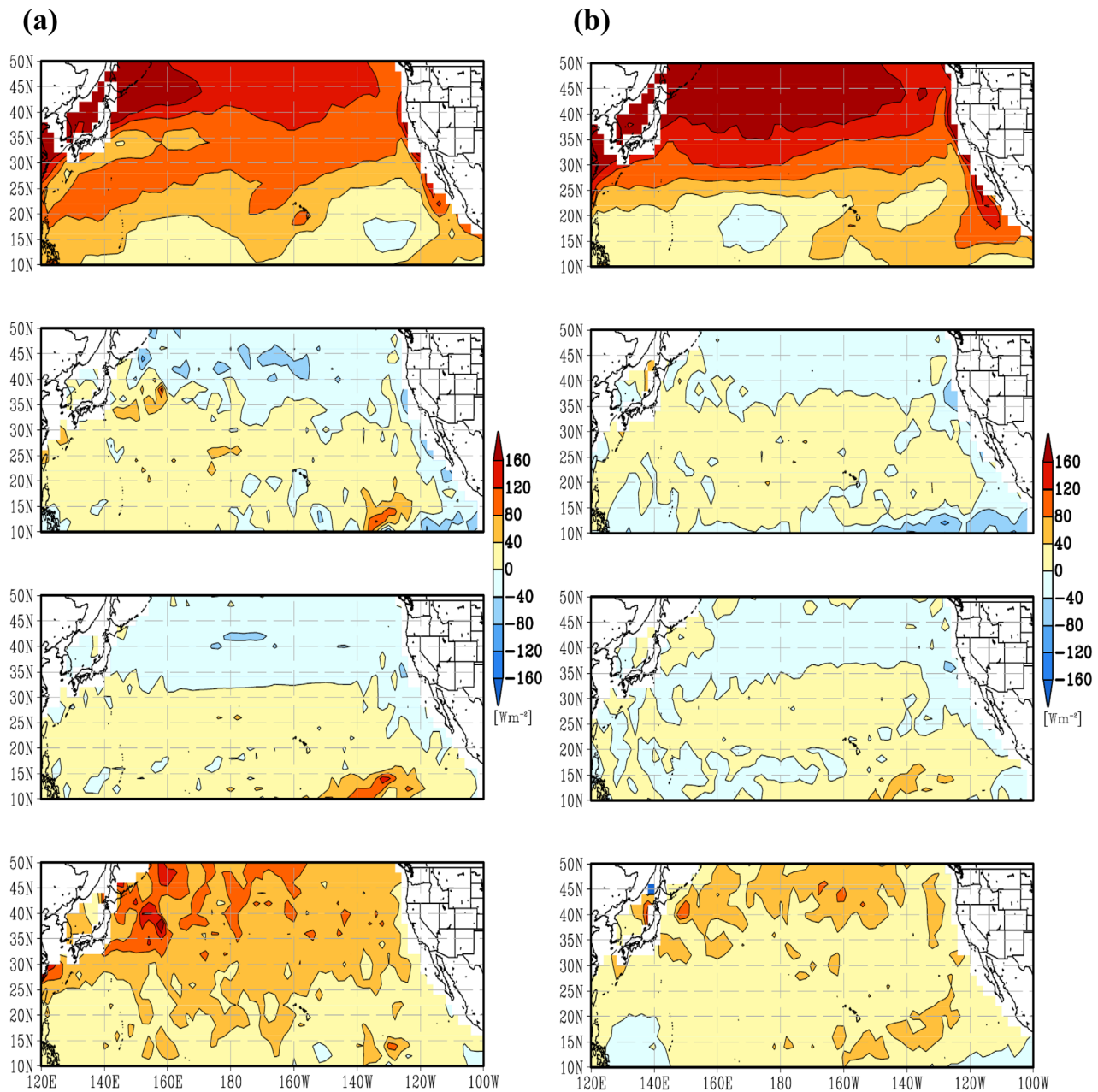


Figure 9. Distributions of heat budget contribution from (top) SHF, (upper middle) OHT, (lower middle) EKA, (bottom) HCV. (a) May and (b) July.

confirms this tendency (Figure 11). It is also found that, in some regions in the low-latitude ocean, where OHT is large and SHF is small,  $Q_h/Q_0$  can be even larger than one.

Table 2. The Domain Averages of the Absolute Values of SHF, OHT, EKA, and HCV

[Wm <sup>-2</sup> ]	May		July	
	$\phi < 30^\circ\text{N}$	$\phi > 30^\circ\text{N}$	$\phi < 30^\circ\text{N}$	$\phi > 30^\circ\text{N}$
$\langle  SHF  \rangle$	55.0	127.1	51.3	156.3
$\langle  OHT  \rangle$	19.9	20.0	18.1	12.5
$\langle  EKA  \rangle$	14.4	9.7	8.3	6.3
$\langle  HCV  \rangle$	32.2	68.3	21.0	37.9

Several mechanisms can be considered for large values of  $Q_h$ . One can expect the contribution from radiation penetration across MLD  $q_h$ , since  $h$  is small. Especially a negative correlation between  $Q_h/Q_0$  and  $h$ , as shown in Figure 11, suggests its contribution in  $Q_h$ . In order to assess

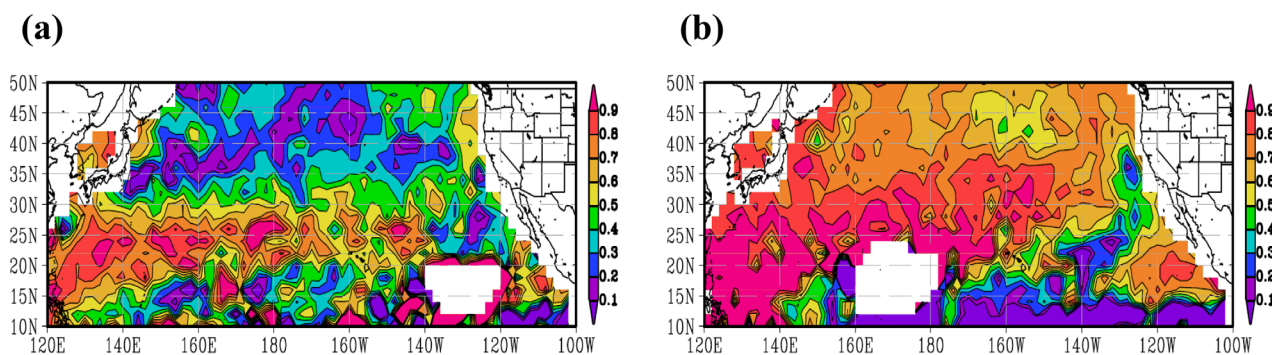


Figure 10. Distributions of  $Q_h/Q_0$  (Blank areas are the regions with negative  $Q_0$ , as observed in Figure 2). (a) May and (b) July.

its contribution, we consider two different types of radiation penetration, i.e., waters of type 1a and 2 from Paulson and Simpson [1977], as in Vivier et al. [2002]. Figure 12 shows the distributions of  $q_h/Q_h$  for both water types. Here the regions with  $Q_h/Q_0 < 0.1$  are not included, which is regarded as the region without significant heat flux across the MLD. The contribution of radiation penetration to  $Q_h$  is important in the low latitude; for example,  $q_h/Q_h > 0.5$  when water type 1a is assumed. On the other hand, in the high-latitude ocean  $q_h/Q_h$  is much smaller than one, regardless of water type. It implies the existence of other processes contributing to  $Q_h$ . The existence of other processes can also be inferred from the fact that the penetration depth of surface heat flux continues to increase with time to the depth beyond solar radiation penetration (Figure 1b).

One can also expect various sources of turbulence below the ML, including internal wave breaking and subsurface shear. Turbulence, and thus vertical mixing, is found to be maintained at a certain level at the seasonal thermocline during summer [e.g., Gregg 1987]. In addition, entrainment arising from day-to-day changes of MLD under the high-frequency variation of atmospheric forcing can also contribute to  $Q_h$ , if the heat budget is calculated based on the monthly MLD [Alexander et al., 2000; Vivier et al., 2002; Qu, 2003]. Qiu et al. [2006] and Cronin et al. [2013] observed a large amount of heat flux across the MLD in the Recirculation Gyre of the Kuroshio Extension region, either from the monthly Argo data [Qiu et al., 2006] or from the daily field observation data [Cronin et al., 2013], and they attributed it to the enhanced diffusivity due to large inertial shear generated by wind events associated with tropical cyclones. It illustrates the

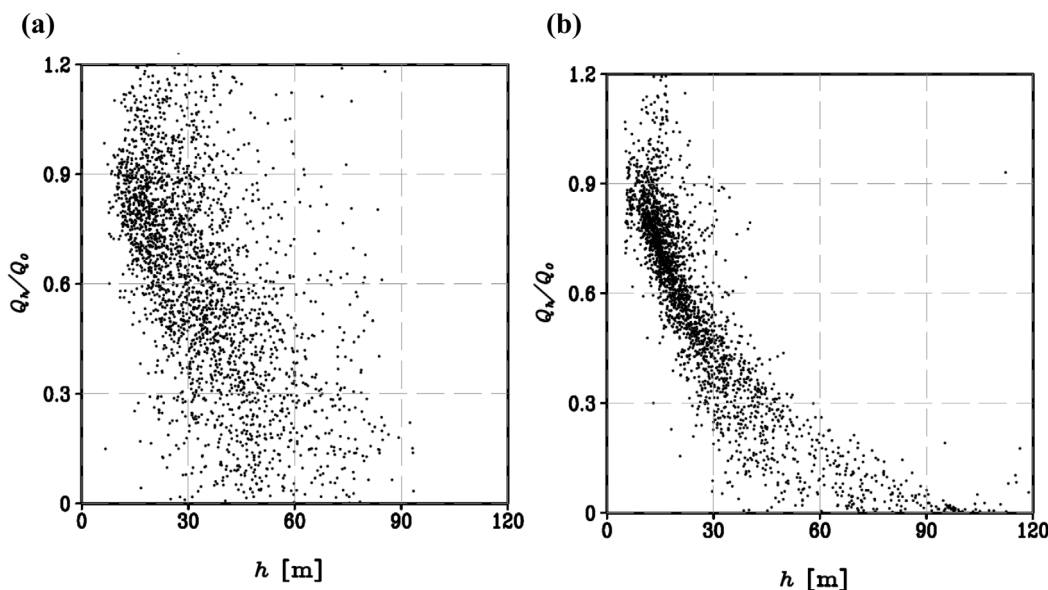


Figure 11. Scatter plots between  $Q_h/Q_0$  and  $h$  (Data with  $Q_0 < 0$  and  $Q_h < 0$  are excluded.). (a)  $\phi < 30^\circ\text{N}$  and (b)  $\phi > 30^\circ\text{N}$ .

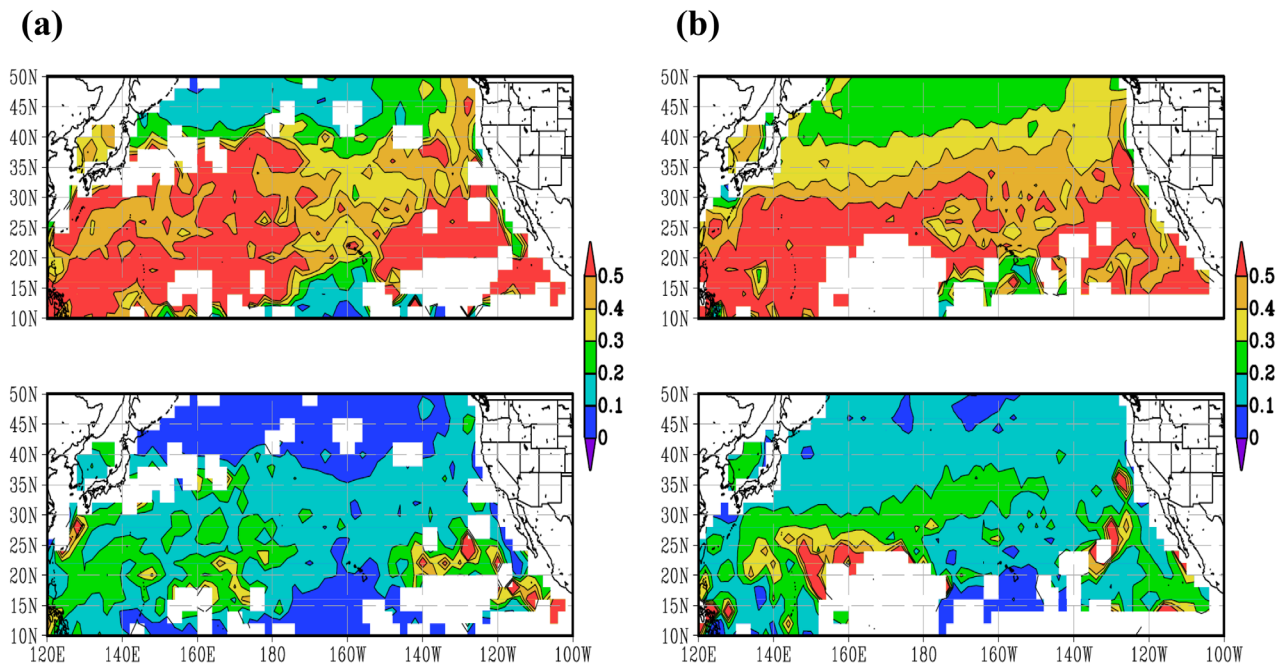


Figure 12. Distributions of  $q_h/Q_h$  from (top) water type 1a and (bottom) water type 2 (Blank areas are the regions with  $Q_h/Q_0 < 0.1$ ). (a) May and (b) July.

contributions of both turbulent transport to below the MLD and the entrainment arising from day-to-day changes of MLD.

Neither the turbulent transport to below the MLD nor the day-to-day changes of MLD arising from the high-frequency atmospheric forcing are resolved in the ocean general circulation model (OGCM) and thus must be parameterized in terms of the vertical mixing coefficient below the MLD  $K_v$ . Figure 13 shows the distributions of  $K_v$  for each water type, which is calculated by using the relation  $K_v \partial B / \partial z = Q_h - q_h$ .  $K_v$  was not calculated in the region with  $q_h/Q_h > 0.9$ , assuming that the contribution by turbulent mixing is

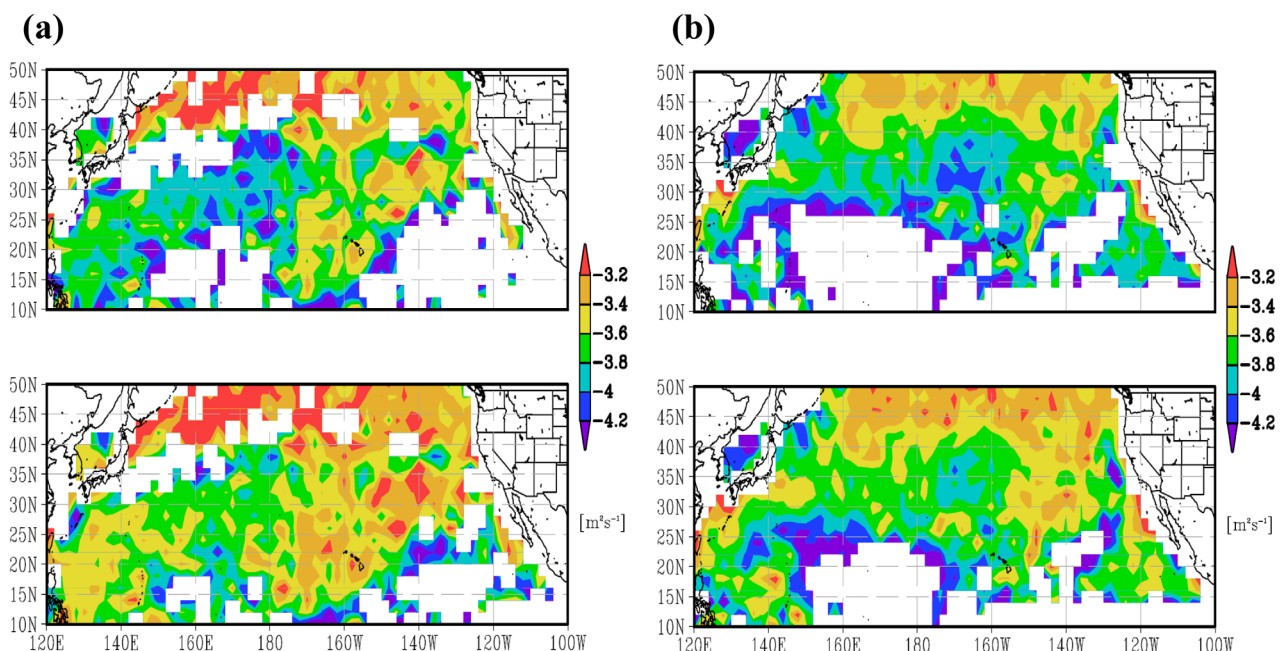


Figure 13. Distributions of  $\log(K_v)$  from (top) water type 1a and (bottom) water type 2 (Blank areas are the regions with  $q_h/Q_h > 0.9$ ). (a) May and (b) July.

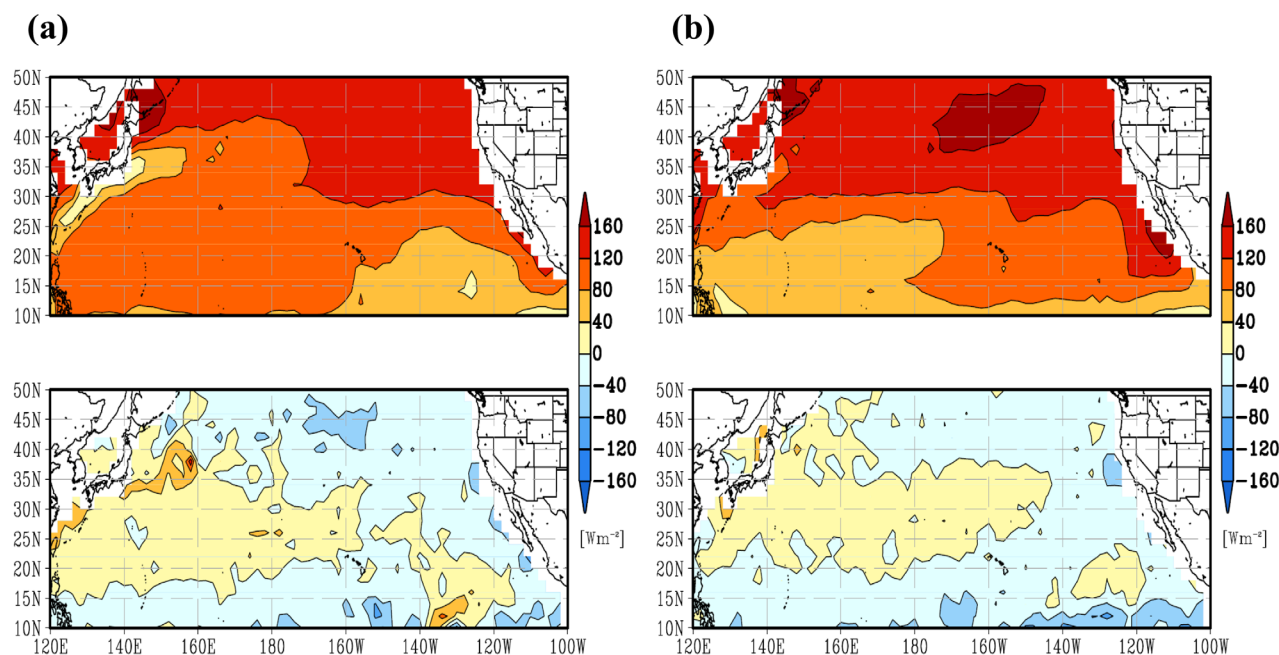


Figure 14. Distributions of heat budget contribution from (top) SHF and (bottom) OHT from OAFlex data. (a) May and (b) July.

insignificant. The value of  $K_v$  in the high-latitude ocean in July is estimated as  $K_v \sim 10^{-4} - 10^{-3} \text{ m}^2 \text{ s}^{-1}$ , which is comparable to the estimations by Qiu *et al.* [2006], Cronin *et al.* [2013], and Hosoda *et al.* [2015].

Note that bulk mixed layer models [Kraus and Turner, 1967; Gaspar, 1988], which is widely used for the heat budget analysis in the upper ocean [Qiu and Kelly, 1993; Yasuda *et al.*, 2000; Vivier *et al.*, 2002; Qu, 2003; Kelly, 2004; Dong *et al.*, 2007; Kako and Kubota, 2009], usually assume  $Q_h - q_h = 0$  during the heating season, if wind stress and surface heat flux do not change with time. The present result suggests that the prediction based on the assumption of  $Q_h - q_h = 0$  can overestimate the increase of SST  $\Delta T_5$  substantially, especially when  $h$  is small.

### 3.5. Sensitivity to Surface Heat Flux Data

Since the surface heat flux plays an important role in the estimation of the present results, such as OHT and  $Q_h$ , it is important to examine how the present results are affected by the surface heat flux data. For this purpose, analysis is repeated by using the heat flux data from the OAFlex data. Figures 14 and 15 show the distributions of heat budget contribution and  $Q_h/Q_0$  from the OAFlex data, corresponding to Figures 9 and 11.

The OAFlex data in Figure 14 shows larger SHF in the low-latitude ocean, and thus smaller latitudinal variation than the NCEP-1 data. Yu *et al.* [2004] suggested that the NCEP-1 data tend to overestimate low-level clouds, and thus leading to the underestimation of solar radiation. As a result, OHT in the low-latitude ocean ( $\phi < 30^\circ\text{N}$ ) tends to be more negative compared to the case in Figure 9, although the magnitude is small in

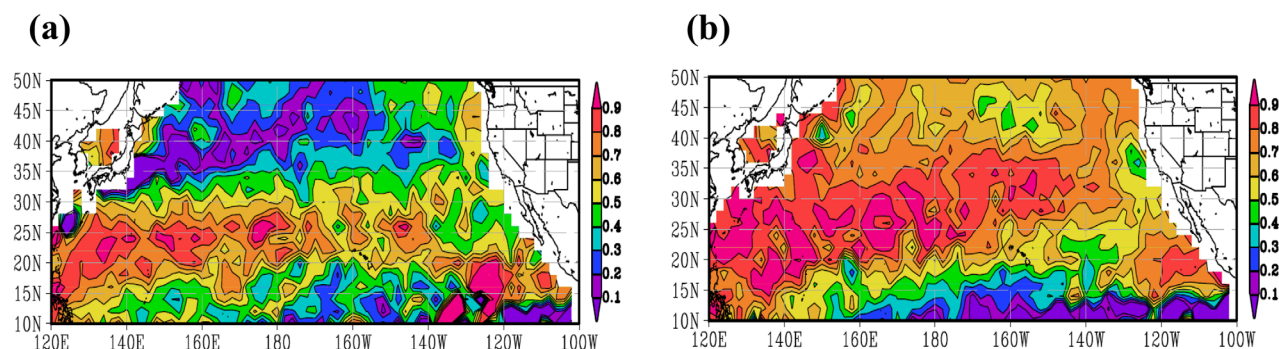
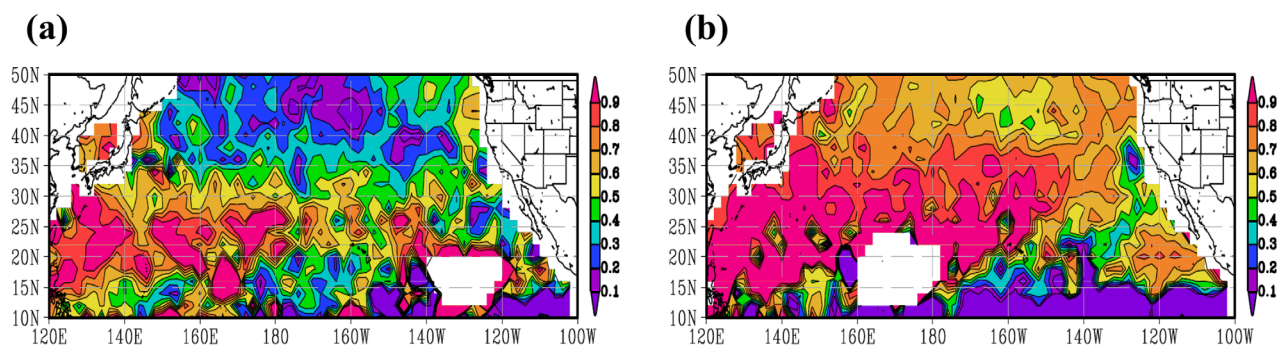


Figure 15. Distributions of  $Q_h/Q_0$  from OAFlex data (Blank areas are the regions with negative  $Q_0$ , as observed in Figure 14). (a) May and (b) July.



**Figure 16.** Distributions of  $Q_h/Q_0$  with the reduced ocean heat transport below the MLD ( $\alpha = 0.5$ ) (Blank areas are the regions with negative  $Q_0$ , as observed in Figure 2). (a) May and (b) July.

both cases of data. Larger SHF also leads to larger  $Q_h$  in the low-latitude ocean. On the other hand, the distribution of OHT in the high-latitude ocean ( $\phi > 30^\circ\text{N}$ ) is not significantly modified. For example, the domain averaged  $|\text{OHT}|$  in May and July, corresponding to Table 2, are about 17.5% and 8.6% of  $|\text{SHF}|$  in the high-latitude ocean, and 21.4% and 23.9% of  $|\text{SHF}|$  in the low-latitude ocean.

The general pattern of the distributions of  $Q_h/Q_0$  remains similar to those from NCEP-1 data, but the region with  $Q_h/Q_0 < 0.1$  becomes smaller in the low-latitude ocean (Figure 15).

### 3.6. Sensitivity to the Uncertainty of OHT

In the present work, the heat budget of the mixed layer during summer has been estimated for the first time without resorting to the model. For this purpose, we assumed that the downward penetration of the surface heat flux is limited to  $z = 100$  m and the contributions from geostrophic advection and lateral mixing are uniform vertically up to  $z = 100$  m. In order to assess the present results properly, it may be necessary to estimate how  $Q_h$  is affected by this assumption.

If the ocean heat transport decreases with depth, (5) can be generalized to

$$\text{OHT} = \frac{h}{\alpha z_H + (1-\alpha)h} (\text{OHT}_{zH} - \text{EKA}) + \text{EKA}, \quad (6)$$

where  $\alpha$  is the ratio of the mean value of  $F$  below the MLD ( $h > z < z_H$ ) to that above the MLD ( $0 < z < h$ ) in (3). The assumption in the present work corresponds to  $\alpha = 1$ .

In order to examine how  $Q_h$  is affected by  $\alpha$ , we consider the case with a sufficiently small  $\alpha$ ; that is,  $\alpha = 0.5$ . When OHT is calculated with  $\alpha = 0.5$  in (6), there is a slight increase of  $Q_h/Q_0$  in the western side of the low-latitude ocean, which is affected by the Kuroshio (Figure 16). It means that the heat flux across the MLD becomes even larger with  $\alpha = 0.5$ . We can regard that  $Q_h/Q_0$  from  $\alpha = 1$  (Figure 10) represents the minimum estimation, although it is close to the real value, while the difference of  $Q_h/Q_0$  between the cases with  $\alpha = 0.5$  and 1 indicates the level of uncertainty.

In the high-latitude ocean, OHT is much smaller than SHF, and thus  $Q_h$  is not expected to be affected significantly by the accuracy of OHT except near the Kuroshio region. On the other hand, SHF and OHT are often comparable in the low-latitude ocean. The comparison with the OAFflux data also reveals the uncertainty of SHF in the low-latitude ocean (Figure 14). These factors can make the estimation of  $Q_h$  in the low-latitude ocean less reliable. Nonetheless, it is important to notice that the main conclusions of the present paper, such as the estimations of  $Q_h$  and  $K_v$ , mainly concern the high-latitude ocean.

## 4. Conclusion and Discussion

In the present paper, we attempt to understand how much SST increases responding to surface heating. For this purpose, we investigate the MLD, the heat budget of the ML, and the heat flux across the MLD during the heating season in the North Pacific ( $10^\circ\text{N} - 50^\circ\text{N}$ ) by analyzing Argo and NCEP-1 data.

Analysis reveals that the response of the upper ocean to surface heating shows different patterns depending on whether it is in the high-latitude ocean ( $\phi > 30^\circ\text{N}$ ) or in the low-latitude ocean ( $\phi < 30^\circ\text{N}$ ), and

whether it is during the early heating period (April–June) or during the late heating period (June–August). The different dynamical processes are due to the contrast in atmospheric forcing and the preexisting stratification in the ocean. In the high-latitude ocean north of 30°N, where a seasonal thermocline is formed from the deep winter mixed layer under strong surface heating, the MLD  $h$  is found to be scaled as  $h \propto (L\lambda)^{1/2}$  during the early heating period, where  $L$  is the Monin-Obukhov length scale and  $\lambda$  is the Ekman length scale. On the other hand, in the low latitude south of 30°N, where the preexisting MLD is shallow and the surface heating is weak,  $h$  is found to be scaled by  $\lambda$  over the whole heating period.

The heat budget of the mixed layer shows that the ocean heat transport (OHT) is much smaller than the surface heat flux (SHF) except near the Kuroshio region in the high-latitude ocean. On the other hand, in the lower latitude, where SHF is small, OHT is often comparable to SHF. The heat flux across the MLD  $Q_h$  becomes significant, when  $h$  is small. Especially  $Q_h/Q_0$  is larger than 0.5 during the late heating period in most regions of the high-latitude ocean. It is found that  $Q_h$  cannot be explained in terms of radiation penetration only, especially in the high-latitude ocean, and turbulent mixing across the MLD must play an important role. The estimation of eddy diffusivity  $K_v$  in the high-latitude ocean  $K_v \sim 10^{-4}–10^{-3} \text{ m}^2 \text{ s}^{-1}$  is consistent with previous estimations [Qiu *et al.*, 2006, Cronin *et al.*, 2013].

The present analysis does not support two important implications in the Kraus and Turner [1967] model, which is widely used for the heat budget analysis in the upper ocean; that is, the depth of a seasonal thermocline proportional to the Monin-Obukhov length scale ( $h \propto L$ ) and no heat flux across the MLD under surface heating ( $Q_h - q_h = 0$ ).

Sensitivity tests were carried out in order to investigate the effects of uncertainty in the SHF data and in the method of calculating OHT. It was found that the main conclusions of the present paper, such as the estimations of  $Q_h$  and  $K_v$  in the high-latitude ocean, are not affected significantly by this uncertainty. Nonetheless, it is important to improve the accuracy of SHF and OHT in the future study. Especially recent reanalysis products, which aim to improve the NCEP-1 data, can be utilized, such as CFSR from NCEP [Saha *et al.*, 2010], ERA-Interim from ECMWF [Dee *et al.*, 2011], MERRA from NASA [Rienecker *et al.*, 2011], and JRA-25 from JMA [Onogi *et al.*, 2007].

In spite of its importance in the coupled ocean-atmosphere system, there still exist relatively few investigations of the dynamical process or the heat budget of the summer mixed layer. We hope that further investigations in the future can quantify various uncertainties, such as the variability of MLD, the heat flux across the base of the ML, and its relation to the upper ocean dynamics, possibly with the help of the ocean model. It will also be interesting to examine how the response of the upper ocean to surface heating, proposed in the present work, plays a role in summer-time air-sea interaction and climate variation.

#### Acknowledgments

This study was supported by the National Research Foundation of Korea grant funded by the Korean Government (MEST) (NRF-2009-C1AAA001-0093068). The data used to produce the results in the present paper are available for free from the corresponding author (noh@yonsei.ac.kr).

#### References

- Alexander, M. A., J. D. Scott, and C. Deser (2000), Processes that influence sea surface temperature and ocean mixed layer depth variability in a coupled model, *J. Geophys. Res.*, *105*, 16,823–16,842.
- Alexander, R. C., and J.-W. Kim (1976), Diagnostic model study of mixed-layer depths in the summer North Pacific, *J. Phys. Oceanogr.*, *6*, 293–298.
- Argo Science Team (2001), The global array of profiling floats, in *Observing the Oceans in the 21st Century*, edited by C. J. Koblin and N. R. Smith, pp. 248–258, Global Ocean Data Assimilation Experiment (GODAE), Proj. Off. and Bureau of Meteorol., Melbourne.
- Carton, J. A., S. A. Grodsky, and H. Liu (2008), Variability of the oceanic mixed layer, 1960–2004, *J. Clim.*, *21*, 1029–1047.
- Cronin, M. F., N. A. Bond, J. T. Farrar, H. Ichikawa, S. R. Jayne, Y. Kawai, M. Konda, B. Qiu, L. Rainville, and H. Tomita (2013), Formation and erosion of the seasonal thermocline in the Kuroshio Extension recirculation gyre, *Deep Sea Res., Part II*, *85*, 62–74.
- de Boyer Montégut, C., G. Madec, A. S. Fischer, A. Lazar, and D. Ludicone (2004), Mixed layer depth over the global ocean: An examination of profile data and a profile-based climatology, *J. Geophys. Res.*, *109*, C12003, doi:10.1029/2004JC002378.
- Dee, D. P., *et al.* (2011), The ERA-Interim reanalysis: Configuration and performance of the data assimilation system, *Q. J. R. Meteorol. Soc.*, *137*, 553–597.
- Deser, C., M. A. Alexander, and M. S. Timlin (1996), Upper-ocean thermal variations in the North Pacific during 1970–1991, *J. Clim.*, *9*, 1840–1855.
- Dong, S., S. T. Gille, and J. Sprintall (2007), An assessment of the Southern Ocean mixed layer heat budget, *J. Clim.*, *20*, 4425–4442.
- Elsberry, R. L., T. S. Fraim, and R. N. Trapnel (1976), A mixed layer model of the oceanic thermal response to hurricanes, *J. Geophys. Res.*, *81*, 1153–1162.
- Garwood, R. W. (1977), An oceanic mixed layer model capable of simulating cyclic states, *J. Phys. Oceanogr.*, *7*, 455–468.
- Gaspar, P. (1988), Modeling the seasonal cycle of the upper ocean, *J. Phys. Oceanogr.*, *18*, 161–180.
- Goh, G., and Y. Noh (2013), Influence of the Coriolis force on the formation of a seasonal thermocline, *Ocean Dyn.*, *63*, 1083–1092.
- Gregg, M. C. (1987), Diapycnal mixing in the thermocline: a review, *J. Geophys. Res.*, *92*, 5249–5286.
- Hao, J., Y. Chen, F. Wang, and P. Lin (2012), Seasonal thermocline in the China Seas and northwestern Pacific Ocean, *J. Geophys. Res.*, *117*, C02022, doi:10.1029/2011JC007246.

- Holte, J. W., L. D. Talley, T. K. Chereskin, and B. M. Sloyan (2012), The role of air-sea fluxes in Subantarctic Mode Water formation, *J. Geophys. Res.*, *117*, C03040, doi:10.1029/2011JC007798.
- Hosoda, S., T. Ohira, K. Sato, and T. Suga (2010), Improved description of global mixed-layer depth using Argo profiling floats, *J. Oceanogr.*, *66*, 773–787.
- Hosoda, S., M. Nonaka, T. Tomita, B. Taguchi, H. Tomita, and N. Iwasaka (2015), Impact of downward heat penetration below the shallow seasonal thermocline on the sea surface temperature, *J. Oceanogr.*, *46*, 1–16, doi:10.1007/s10872-015-0275-7.
- Imawaki S., H. Uchida, H. Ichikawa, M. Fukusawa, S. Umatani, and the ASUKA Group (2001), Satellite altimeter monitoring the Kuroshio transport south of Japan, *Geophys. Res. Lett.* *28*, 17–20.
- Kagimoto, T., and T. Yamagata (1997), Seasonal transport variation of the Kuroshio: An OGCM simulation, *J. Phys. Oceanogr.*, *27*, 403–418.
- Kalnay, E., et al. (1996), The NCEP/NCAR 40-year reanalysis project, *Bull. Am. Meteorol. Soc.*, *77*, 437–472.
- Kako, S., and M. Kubota (2009), Numerical study on the variability of mixed layer temperature in the North Pacific, *J. Phys. Oceanogr.*, *39*, 737–752.
- Kang, Y. J., Y. Noh, and S.-W. Yeh (2010), Processes that influence the mixed layer deepening during winter in the North Pacific, *J. Geophys. Res.*, *115*, C12004, doi:10.1029/2009JC005833.
- Kara, A. B., P. A. Rochford, and H. E. Hurlburt (2003), Mixed layer depth variability over the global ocean, *J. Geophys. Res.*, *108*, C33079, doi:10.1029/2000JC000736.
- Kelly, A. K. (2004), The relationship between oceanic heat transport and surface fluxes in the western North Pacific: 1970–2000, *J. Clim.*, *17*, 573–588.
- Kraus, E. B., and J. S. Turner (1967), A one-dimensional model of the seasonal thermocline II. The general theory and its consequences, *Tellus*, *19*, 98–105.
- Liu, Q., S. P. Xie, L. Li, and N. A. Maximenko (2005), Ocean thermal advective effect on the annual range of sea surface temperature, *Geophys. Res. Lett.*, *32*, L24604, doi:10.1029/2005GL024493.
- Lozovatsky, I., M. Figueroa, E. Roget, H. J. S. Fernando, and S. Shapovalov (2005), Observations and scaling of the upper mixed layer in the North Atlantic, *J. Geophys. Res.*, *110*, C05013, doi:10.1029/2004JC002708.
- Nieuwstadt, F. T. M. (1984), The turbulent structure of the stable, nocturnal boundary layer, *J. Atmos. Sci.*, *41*, 2206–2216.
- Noh, Y., and W. S. Lee (2008), Prediction of the mixed and mixing layer depths from an OGCM, *J. Oceanogr.*, *64*, 217–225.
- Ohno, Y., T. Kobayashi, N. Iwasaka, and T. Suga (2004), The mixed layer depth in the North Pacific as detected by the ARGO, *Geophys. Res. Lett.*, *31*, L11306, doi:10.1029/2004GL019576.
- Ohno, Y., N. Iwasaka, F. Kobashi, and Y. Sato (2009), Mixed layer depth climatology of the North Pacific based on Argo observations, *J. Oceanogr.*, *65*, 1–16.
- Onogi, K., et al. (2007), The JRA-25 reanalysis. *J. Meteorol. Soc. Jpn.*, *85*, 369–432.
- Paulson, C. A. and J. J. Simpson (1977), Irradiance measurements in the upper ocean, *J. Phys. Oceanogr.*, *7*, 952–956.
- Pollard, R. T., P. B. Rhines, and R. O. R. Y. Thompson (1973) The deepening of the wind-mixed layer. *J. Geophys. Fluid Dyn.*, *3*, 381–404.
- Qiu, B., and S. Chen (2005), Eddy-induced heat transport in the subtropical North Pacific from Argo, TMI, and altimetry measurements, *J. Phys. Oceanogr.*, *35*, 458–473.
- Qiu, B., and K. A. Kelly (1993), Upper ocean heat balance in the Kuroshio Extension region, *J. Phys. Oceanogr.*, *23*, 2027–2041.
- Qiu, B., S. Chen, and P. Hacker (2004), Synoptic-scale air-sea flux forcing in the western North Pacific: Observations and their impact on SST and the mixed layer, *J. Phys. Oceanogr.*, *34*, 2148–2159.
- Qiu, B., P. Hacker, S. Chen, K. A. Donohue, D. R. Watts, H. Mitsudera, N. G. Hogg, and S. R. Jayne (2006), Observations of the subtropical mode water evolution from the Kuroshio Extension System Study, *J. Phys. Oceanogr.*, *36*, 457–473.
- Qu, T. (2003), Mixed layer heat balance in the western North Pacific, *J. Geophys. Res.* *108*(C7), 3242, doi:10.1029/2002JC001536.
- Resnyanskiy, Y. D. (1975), Parameterization of the integral turbulent energy dissipation in the upper quasi homogeneous layer of the ocean, *Izv. Atmos. Ocean. Phys.*, *11*, 453–457.
- Rienecker, M. M., et al. (2011), MERRA: NASA's modern-era retrospective analysis for research and application, *J. Clim.*, *24*, 3624–3647.
- Saha, S., et al. (2010), The NCEP climate forecast system reanalysis, *Bull. Am. Meteor. Soc.*, *91*, 1015–1057.
- Schneider, N., and P. Müller (1990), The meridional and seasonal structures of the mixed-layer depth and its diurnal amplitude observed during the Hawaii-to-Tahiti shuttle experiment, *J. Phys. Oceanogr.*, *20*, 1395–1404.
- Tomita, T., S.-P. Xie, and M. Nonaka (2002), Estimates of surface and subsurface forcing for decadal sea surface temperature variability in the mid-latitude North Pacific, *J. Meteorol. Soc. Jpn.*, *80*, 1289–1300.
- Vivier, F., K. A. Kelly, and L. Thompson (2002), Heat budget in the Kuroshio Extension region: 1993–99, *J. Phys. Oceanogr.*, *32*, 3436–3454.
- Wells, N. C. (1979), A coupled ocean-atmosphere experiment: The ocean response, *Q. J. R. Meteorol. Soc.*, *31*, 1297–1307.
- Yasuda, I., T. Tozuka, M. Noto, and S. Koutetsu (2000), Heat balance and regime shifts of the mixed layer in the Kuroshio Extension, *Prog. Oceanogr.*, *47*, 257–278.
- Yim, B. Y., Y. Noh, B. Qiu, S. H. You, and J. H. Yoon (2010), The vertical structure of eddy heat transport simulated by an eddy-resolving OGCM, *J. Phys. Oceanogr.*, *40*, 340–353.
- Yoshikawa, Y. (2015), Scaling surface mixing/mixed layer depth under stabilizing buoyancy flux, *J. Phys. Oceanogr.*, *45*, 247–258.
- Yu, L., R. A. Weller, and B. Sun (2004), Improving latent and sensible heat flux estimates for the Atlantic Ocean, *J. Clim.*, *17*, 373–393.
- Yu, L., X. Jin, and R. Weller (2006), Role of net surface heat flux in seasonal variations of sea surface temperature in the tropical Atlantic Ocean, *J. Clim.*, *19*, 6153–6169.
- Zillitinkovich, S., I. Esau, and A. Baklanov (2007), Further comments on the equilibrium height of neutral and stable planetary boundary layers, *Q. J. R. Meteorol. Soc.*, *133*, 265–271.